JOURNAL OF THERMOPHYSICS AND HEAT TRANSFER
Vol. 9, No. 3, July–September 1995

Mass Spectrometric and Electrostatic Probe Measurements of N_2/O_2 Plasma Flow

P. Asselin,* S. Cayet,* P. Lasgorceix,† V. Lago,* and M. Dudeck‡
Centre Nationale de la Recherche Scientifique, 92190 Meudon, France

Plasma wind tunnels are used at the Laboratoire d'Aérothermique at Meudon to simulate the different parameters of the gas surrounding the surface of space vehicles during hypersonic flight in the upper atmosphere. In the present work, mass spectrometric and double electrostatic probe measurements in a stagnation point are performed in N_2/O_2 plasmas. Axial distributions of electron density and temperature are obtained from the fit between experimental data and Laframboise expression for the double cylindrical probe current. Neutral and ion distributions are measured by mass analysis for different axial positions, and are then compared with a chemical model for air, in order to evaluate the dominant reactions in the plasma flow.

Nomenclature

F	=	scalar expression defined as the difference between experimental and theoretical double-probe currents
H_{exp}, H_{th}	=	experimental and theoretical double-probe currents
I_s, V_s	=	current, voltage probes
J_k	=	measured current by a collector area for a species k
l, d, A	=	length, diameter, and area of sampling orifice
N_e	=	electron density
n_k, v_k	=	density, thermal velocity of the species k
r, A_k	=	probe radius and area
T_e	=	electron temperature
T_r, T_v	=	rotational, vibrational temperatures
v	=	plasma flow velocity
w_j	=	production rate relative to the reaction j
z	=	axial coordinate of position vector
λ_D	=	Debye length
λ_n, λ_i	=	neutral mean free path, ion mean free path
θ_d	=	dissociation coefficient of a molecular species

Introduction

PLASMA wind tunnels are used to simulate space vehicle atmospheric re-entry conditions with large continuous plasma jets of high specific enthalpies at low pressures, making them an ideal tool for developing spacecraft thermal protection materials.[1,2] Significant heat transfer also occurs behind the shock layer created upstream of the vehicle. This modifies considerably the nature and the composition of the plasma, and much research is currently in progress on the aerothermodynamics and chemistry of these gaseous flows.[3–8]

The Laboratoire d'Aérothermique is equipped with three plasma wind tunnels (dubbed SR1, SR5, and SR6), in which low-pressure arcjets are generated to simulate certain parameters of the gas surrounding the surface of a vehicle during hypersonic re-entry (above 60 km up from the Earth's surface). Several blown-arc plasma generators have been developed that use a great variety of gases, such as argon, hydrogen, nitrogen, air, or mixtures corresponding to particular planetary atmospheres such as CO_2 (Mars) and N_2-CH_4 (Titan). Different experimental methods are currently used to characterize the properties of the plasma jets. With optical emission spectroscopy, rotational and vibrational temperatures of excited levels can be deduced at the nozzle exit from the $\Delta v = 0$ transitions of the first negative spectrum of N_2^+, up to 50 cm downstream from the $\Delta v = 0$ transitions of the violet spectrum of CN by comparison with a calculated spectrum.[8] Intrusive techniques as pitot probes, heat flux probes,[9] electrostatic probes, and mass spectrometry[10] are investigated to study specific plasma conditions. These last two diagnostics have been significantly modified and will be described in detail in the present work. First, some measurements were made at a stagnation point within an air plasma. Some electron density and temperature data will be presented, as obtained by double electrostatic probes, along with the molar fraction of neutrals and ions analyzed by mass spectrometry. Finally, mass spectrometric measurements will be compared with a chemical model for air.

Experimental

Plasma Generator

Our experiments are performed in a cylindrical steel vacuum chamber, 1 m in diameter and 2.3 m long. Vacuum conditions are obtained by a Roots pump group with a flow rate of 20,000 $m^3 \cdot h^{-1}$ at a pressure of 5.10^{-2} torr. A static pressure around 10^{-1} torr is typically reached with a plasma mass flow rate of 0.2 $g \cdot s^{-1}$. Figure 1 shows the general scheme of the experimental setup in the SR1 plasma wind tunnel. Continuous plasma jets are generated by an arc discharge. An electric arc is created between the tip of a copper cathode crossed by a zirconium insert, 2 mm in diameter, and the neck of a copper nozzle (4 mm in diameter), both cooled by a water circuit. The arc is started by a high-frequency high-voltage discharge (6000 V) between the nozzle and the zirconium cathode, and is maintained by a power supply of regulated intensity with an operating range of 70 V/500 A. The electrodes are insulated electrically from each other by an insulator (Celoron®), and the generator chamber is protected thermally by a piece of ceramic. The arc is rotated by the vortex motion of the gas injected into the arc chamber. The plasma generator used for our application offers the possibility of forming the plasma by the electric arc from the direct injection of a N_2-O_2 mixture into the generating chamber. In practice, this produces air plasma jets characterized by low fluctuations of the arc potential (<1%) and a lifetime of several hours for airflows between 10–20 slm and arc currents

Received Feb. 3, 1994; revision received Nov. 10, 1994; accepted for publication Dec. 8, 1994.

*Research Scientist, Laboratoire d'Aérothermique, 4 ter, Route des Gardes.
†Chargé de Recherches, Laboratoire d'Aérothermique, 4 ter, Route des Gardes.
‡Professor, Université de Paris 6. Member AIAA.

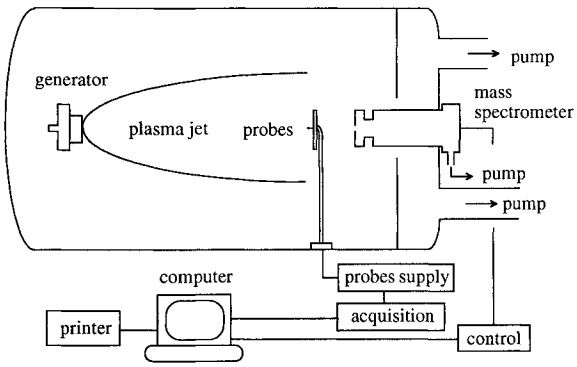

Fig. 1 Diagram of the experimental device in the plasma wind-tunnel SR1.

in the 50–200 A range. For these conditions, generator energy efficiencies are 30–70%, with power supply ranging from 3 to 12 kW. Lastly, high specific enthalpies (10–20 MJ/kg) are available using this arc generator due to the low mass flow rates (0.22 $g \cdot s^{-1}$ for air at 10 slm).

Neutrals and Ion Detection

The mass spectrometer is a standard quadrupole analyzer Balzers QMG 420 consisting of four distinct elements[11]:

1) A cross-beam ion source with its electrostatic optics for detecting neutrals.

2) An ion transfer optics with three metal cylinders and a circular baffle in the middle of the second cylinder, forming two electrostatic lenses to focus the positive and negative ions coming from the plasma (Fig. 2).

3) A quadrupole mass filter consisting of four cylindrical rods in molybdenum, 200 mm long and 8 mm in diameter, used to explore mass ranges between 1–512 amu.

4) A secondary electron multiplier arranged at 90 deg with respect to the analyzer.

The spectrometer housing is connected by a cylindrical ceramic insulating piece to a water-cooled circular flat stainless steel plate 100 mm in diameter, 1 mm thick, and with a 100 μm opening in the center. This large plate is inserted directly in the plasma flow in order to measure the plasma conditions at a stagnation point in front of a catalytic sample material. Plasma particles are sampled through the hole into the spectrometer. This forms with the turbomolecular pump flanged at the exit of the quadrupole mass filter, a differential pumping stage from 10^{-1} torr in front of the orifice down to 10^{-6} torr inside the analyzer. When measuring neutral particles, the transfer optics is set to a repelling potential for positive ions and the cross-beam ion source is switched on. Inversely, when measuring charged particles, suitable voltages are applied to the transfer optics, so that when divergent ions from the plasma are directed around the baffle by the first lens, situated around 5 mm behind the sampling aperture, they are focused on the entrance of the quadrupole mass filter by the second lens. In this latter case, the ion source is switched off.

Electron Density and Temperature Measurement

Electrostatic double probes were used to determine the electron density N_e and temperature T_e close to the surface of a circular flat plate. The device consists of two cylindrical tungsten wires of 200 μm radius and 4 mm length. Each of them is held fixed in an alumina tube about 1 mm in diameter and with a 200 μm channel running through the center. The two alumina tubes are then fitted inside two channels of 1 mm diameter, spaced out 2 mm, passing through a larger alumina tube ($\phi \simeq 4$ mm), and then cemented at each end of the channels. The two probes are first placed as close as possible to an axial position with respect to the plasma flow. They are then inserted in the orifice of a flat plane (with dimensions similar to those of the mass spectrometer), and

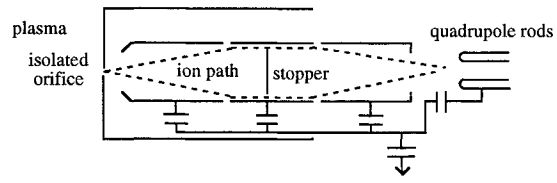

Fig. 2 Diagram of the mass spectrometer ion transfer optics.

mounted at the end of a water-cooled revolving arm in order to prevent damage to the probe device. The probes are polarized by a voltage generator delivering periodic triangular signals with adjustable rise and fall times. The voltage corresponding to the probe current I_s passing through a standard resistance (1, 10, or 100 Ω), the polarization voltage V_s between the two probes, and the arc voltage (to control the stability of the arc during the storage) are sent to an RTI 860 acquisition system (sampling time $\simeq 20$ μs) linked to a computer, which displays the double-probe characteristic $I_s = f(V_s)$. The frequency used for the triangular signal is 100 Hz, hence, the acquisition time corresponding to a half-period is 5 ms and a probe characteristic includes 250 measurement points.

Theory

Concerning the analysis of the neutral and charged particles by mass spectrometry, the length l, the diameter d, and the electric potential of the sampling orifice were chosen in order to be sure that the gas sampled is representative of the plasma chemistry at the entry surface of the plate. Similarly, our electrostatic probe theory is determined by the order of the dimensions of the probe collector element relative to the characteristic parameters of the plasma. In our plasma, the mean free paths of neutrals λ_n and charged particles λ_i are large compared to the Debye length λ_D (collisionless process), and the hole diameter d was decided in consideration of the molecular flow conditions, i.e., the inequality $\lambda_n, \lambda_i >> d > \lambda_D$. The flat plate of the spectrometer is set at a floating potential to limit the electric field penetration through the sampling orifice. Lastly, considering the high aspect ratio (l/d) ($=10$) of the orifice, the measurements presented here include the effects of recombination in front and inside the orifice, so that the relative concentrations of the atomic species are largely underestimated. The classical theory of the probes assumes that the plasma sheath is collisionless and is determined by the radius r of the probes, which is small compared to λ_n and λ_i. From the calculations of the simple probe currents of Laframboise[12] for the Maxwellian electron and ion energy distribution functions, Peterson and Talbot[13] give an algebraic description for the simple probe characteristics, in a region where $\lambda_D < r$. The characteristics of the floating double probes[14] are deduced from those of the simple probes.

Data Analysis

Before presenting our mass spectrometry and double electrostatic probes results, it is important to explain 1) how the raw mass spectrum is corrected to obtain the relative densities of the neutrals and ions; and 2) how the double probe characteristics are analyzed to obtain N_e and T_e.

Mass Spectrometry

The relative densities of the neutral particles and ions are measured differently, because of the cross-beam ion source used for the neutrals. For the dominant neutral particles of the plasma, our data analysis is addressed by the following points:

1) The mass peak currents in the residual vacuum mass spectrum are subtracted from the mass peak currents measured inside the plasma.

2) Knowing that only the current ratios measured with the spectrometer are significant, each current for a given mass is referenced to the dominant peak (N_2 for the neutral particles, NO^+ for the ions). Around this point, it would seem more correct to use some species that is not involved in the plasma chemistry as mass reference for neutrals. For this reason, it is planned to inject a controlled flow of helium gas directly in the mass analyzer.

3) In shock-layer conditions, the effect of the plasma flow velocity near the sampling orifice must not be considered. The current measured by the collector area A for a species k is expressed by

$$J_k = An_k v_k / 2\sqrt{\pi}$$

where n_k is the density and v_k is the thermal velocity of the species k taken at wall conditions. Assuming that all the heavy species have the same temperature, the effective current ratios (J_k/J_l) for two species k and l are linked to the density ratios by the factor $\sqrt{(m_l/m_k)}$.

4) The last point concerns the effect of the cross-beam ion source on the neutral particles. Dissociation reactions induced by the ionization grid inevitably disturb the measurements, and the dissociation coefficient θ_d for each molecular species present in the plasma must be measured, or at least estimated. This estimation was made on the basis of measurements in a neutral gas flow for N_2 and O_2 (θ_d = 0.23 and 0.33, respectively), and of measurements in residual vacuum for H_2 and H_2O (0.34 and 0.33) by extrapolating the dissociation energy of these four molecules as a function of θ_d for NH, OH, NO, and N_2O (two possible dissociation reactions with N_2O). All these points are taken into account to obtain the real relative currents corresponding to the plasma chemistry, and hence, the molar fraction of the neutral species. Only points 2 and 3 of the preceding paragraph apply to the analysis of the ions, considering that no ions are present in the residual vacuum spectrum and that the cross-beam ion source is switched off.

Double Electrostatic Probes

It is possible to apply a nonlinear global optimization to the double-probe characteristics using T_e, N_e, and the area ratio (A_1/A_2) of the probes as parameters. A minimization criterion is defined for the scalar $F = \|H_{th} - H_{exp}\|$, where H_{th} and H_{exp} are the theoretical[15] and experimental double probe currents, respectively. The expression for F is then calculated repeatedly until the convergence criterion chosen is satisfied. Two remarks can be made concerning the use of this algorithm.

1) The method is not sensitive enough to determine the ionic temperature T_i. Nevertheless, if T_i is varied about 50%, the value of N_e changes distinctly (≈20%). In the present case, T_i is taken as the temperature of heavy species, determined by optical emission spectroscopy.[8]

2) By analyzing double-probe characteristics with (A_1/A_2) fixed to unity, the fit is less satisfactory, but yields nearly similar results for N_e and T_e. For this reason (A_1/A_2) was introduced as a fit parameter. It is observed that the area ratio decreases from 0.86 to 0.75 with the z position. From this result, two remarks can be made:

1) The value of (A_1/A_2) (lower than 1) means that the two probes are not quite identical (differences of length, surface condition, angle of attack with respect to the plasma flow, etc.).

2) It is not appropriate to relate the variation of (A_1/A_2) along the z axis with axial changes of one of the three parameters previously cited. Between 200–400 mm, the possible range of the flow impingent angles with respect to both probes (not necessarily parallel between them) is estimated to −20 deg/+20 deg, but the angle between the flow and the z axis is assumed to be zero. Statistical errors in the nonlinear optimization as well as hydrodynamical fluctuations in the plasma must be taken into account to explain this variation of (A_1/A_2) with z.

Results

The results presented are the mass analysis of neutral particles and ions, and the electron density and temperature, determined from double-probe characteristics. In both cases, the measurements are performed in air plasma (100 A, 10 slm) behind (with mass spectrometer) and in front of (with electrostatic probes) a flat plate. Since the plasma generator is mobile along the jet axis z, the distance has been varied in steps of 50 mm, from 400 to 200 mm in the mass analysis case, from 400 to 100 mm in the double probe case. Examples of raw mass spectra are given for neutral particles (Fig. 3) and ions (Fig. 4) at z = 300 mm. Due to their intensity, 10 mass channels (1, 2, 14, 15, 16, 17, 18, 28, 30, 32, 44) are stored in the neutral spectrum, and eight in the ionic spectrum (14, 16, 18, 19, 28, 30, 32, 44). It is difficult a priori to discriminate at the mass 44, N_2O from CO_2 and N_2O^+ from CO_2^+ in both mass spectra of neutrals and ions. However, several arguments play in favor of the presence of N_2O and N_2O^+: firstly, the signal at mass 44 seems to come from the air plasma and not from the residual gas, because we measured a bell-shaped radial profile of the effective peak current, similar to the plasma jet form. Secondly, if CO_2 was detected at the mass 44, we should measure a weak signal at the mass 12 (C) due to the cracking pattern of CO_2, but such a signal has not been detected. After analysis of the data, only eight neutral species (H_2, NH, OH, H_2O, N_2, NO, O_2, N_2O) and seven ions (N^+, O^+, H_2O^+, N_2^+, NO^+, O_2^+, N_2O^+) have molar fractions greater than 10^{-3}. The molar fraction of the neutrals or of the ions is defined with respect to the total sum of the neutrals or of the ions because the acquisition of the mass spectrum for neutrals is independent of that of the ions. The variation of the molar fraction of the neutral species as a function of the axial distance is shown in Fig. 5, and that of the ions in Fig.

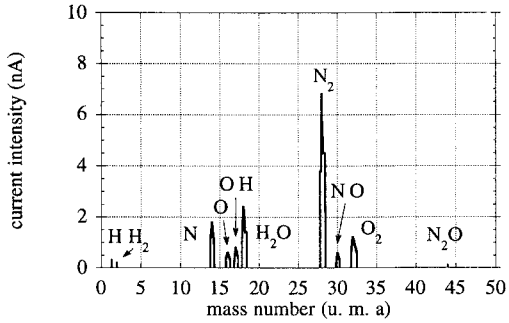

Fig. 3 Mass spectrum of neutral particles in air plasma (10 slm, 100 A) on the jet axis at z = 300 mm.

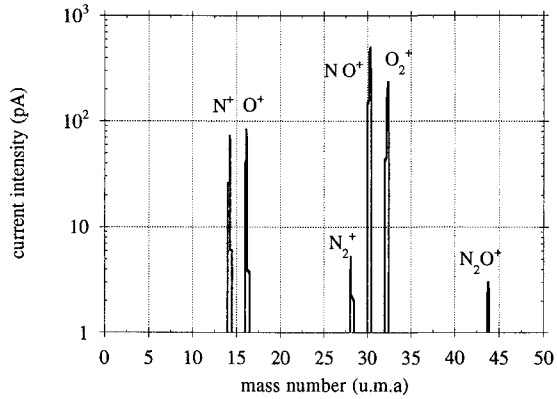

Fig. 4 Mass spectrum of ions in air plasma (10 slm, 100 A) on the jet axis at z = 300 mm.

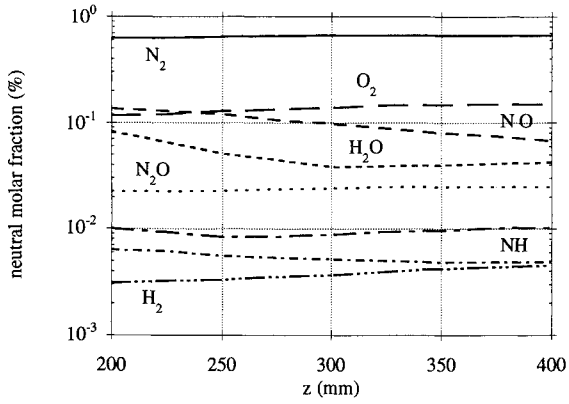

Fig. 5 Neutral particle distribution measured in air plasma between z = 200–400 mm.

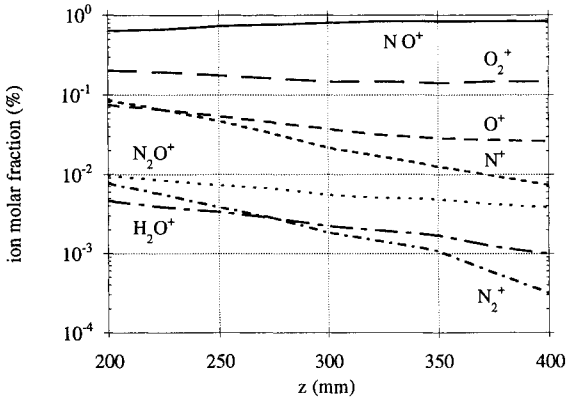

Fig. 6 Ion distribution measured in air plasma between z = 200–400 mm.

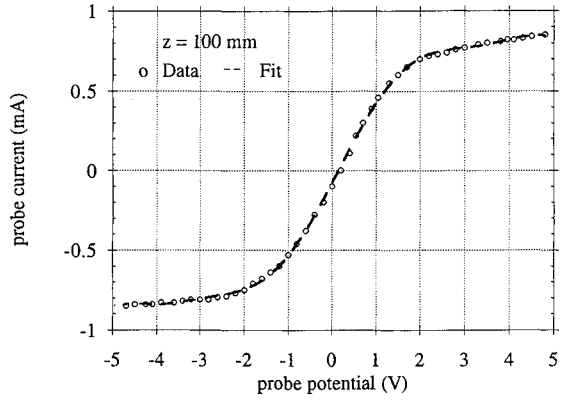

Fig. 7 Experimental double probe characteristic obtained in air plasma at z = 100 mm.

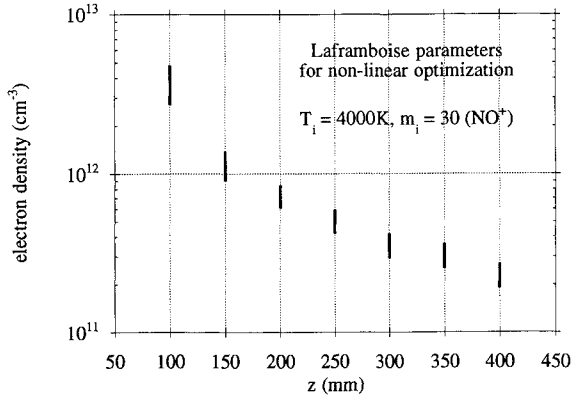

Fig. 8 Electron density vs axial position (100–400 mm) in air plasma on the jet axis. The uncertainty about the determination of N_e is represented by vertical error bars and is estimated to 15%.

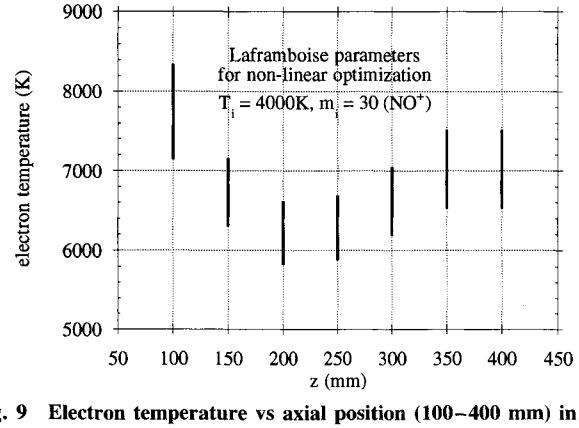

Fig. 9 Electron temperature vs axial position (100–400 mm) in air plasma on the jet axis. The uncertainty about the determination of T_e is represented by vertical error bars and is estimated to 15%.

6. The detection of hydrogenated species in the mass spectra (H_2, NH, OH, H_2O, H_2O^+) is due to the presence of water molecules, which were dissociated or ionized in front of the orifice of the flat plane. It is believed that the absence of neutral atomic species N and O after analysis (lower than 0.1%) is due perhaps to a catalytic reaction between molecular particles and the stainless steel plate and the sampling channel. The absence of neutral atomic oxygen can't be explained by chemical reaction with copper coming from the anode, because the vaporated copper mass is negligible, although optical spectral lines of copper have been observed. Our results can be compared with the particle distribution obtained in the PWK2-IRS plasma wind tunnel by Schönemann et al.[16–18] for N_2-O_2 mixtures. Their plasma conditions differ greatly from ours (56 MJ/kg with an arc current of 1000 A compared with 20 MJ/kg with an arc current of 100 A). Consequently, higher electronic temperatures are obtained (about 12,000 K at z = 260 mm compared with 6000 K in our case). The greater quantity of electron collisions in the PWK2-IRS, as well as the atomic recombination rate enhanced by the catalyticity of our stainless steel plate may explain why the dominant ion observed in their ion distribution is N^+ at the center of the jet and at z = 260 mm,[16] whereas in the present work (Fig. 6), NO^+ is distinctly preponderant.

An experimental double-probe characteristic obtained in front of the stainless steel plate inside the air plasma flow at z = 100 mm is represented in Fig. 7. The solid line is the fit of the double-probe current with the theory of Laframboise.[12] The electron density distribution on the jet axis is shown in Fig. 8. The electron density falls off sharply from z = 100 mm to z = 300 mm (from 4.10^{12} cm^{-3} to 3.5 10^{11} cm^{-3}), which indicates a strong electronic recombination rate. Due to the same type of reaction, N_e decreases more smoothly beyond z = 300 mm. This measurement seems to be inconsistent with the ionic mass spectrum Fig. 6 because the molar fraction of the dominant ion NO^+ increases with z. However, each ion molar fraction presented in Fig. 6 is expressed with respect to the total number of ions. The axial evolution of the absolute density of NO^+ can be approximated from measured values of the ratio between the electron density (Fig. 5) and the total number of species, and of the ratio between the ion molar fractions of NO^+ and O_2^+ (Fig. 6). It is found that the density of NO^+ decreases by about a factor 4 between z = 200 and 400 mm, and it can be concluded that the density of all ionic species decreases with z, as for the electron density.

The electron temperature distribution Fig. 9 is roughly similar to that of the rotational temperature T_r obtained in a N_2-0.1% CH_4 mixture,[8] but T_e always is about 2500 K higher

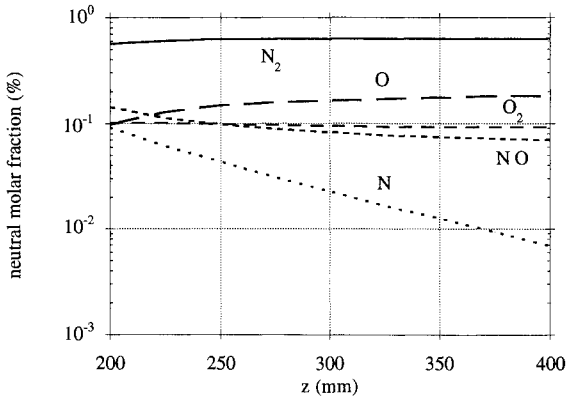

Fig. 10 Calculated molar fractions for the neutral particles in air plasma.

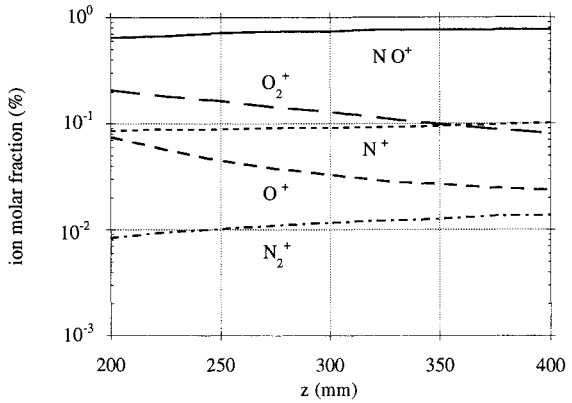

Fig. 11 Calculated molar fractions for the ions in air plasma.

than T_r. The electron temperature decreases sharply on the jet axis, from 7700 to 6200 K between $z = 100$ and 200 mm. Beyond 200 mm and up to 400 mm, the value of T_e increases to 7000 K before decreasing again. This result might be related to the presence of crossed shock layers issuing from the nozzle, which originate successive zones of compression and expansion by reflection on the jet boundaries. This phenomenon has been frequently observed in arc plasma jets about up to 50 mm from the nozzle exit.[19] It is not clear that the increase of T_e observed from $z = 300$ mm is due to pressure oscillations, because in this case, the axial evolution of N_e should be similar. The large uncertainty (estimated to 15% from systematic measurements at a fixed position) about the determination of T_e (Fig. 9) may explain this apparent inconsistency between both results.

Chemical Kinetics

The Park[20,21] model for air is used to compare the usual chemical kinetics with our mass spectrometry measurements, which include recombination effects. The model takes into account 11 particles (N, O, N_2, NO, O_2, N^+, O^+, N_2^+, NO^+, O_2^+, e) and 32 reactions, classified in six types: dissociation with a heavy particle or with an electron, neutral exchange, associative ionization, electron impact ionization, and charge transfer. The system of coupled differential equations for the variation of the molar fractions of 11 particles is solved using a Runge–Kutta method with an adaptive step determined by a convergence test. The molar fraction of the species determined experimentally, as well as the stagnation pressure measured with a pitot tube at $z = 200$ mm, determine the initial conditions needed to start the chemical kinetics. A velocity distribution on the jet axis obtained by time-of-flight measurements in our plasmas[22] is used to convert a time scale into a length scale. Three temperatures are entered in the chemical model: 1) T_r for heavy species, 2) T_e for electrons, and 3) T_v the vibrational temperature. These are assumed to remain constant throughout the chemical process. The numerical simulation results are presented separately for the neutral particles (Fig. 10) and for the ions (Fig. 11). The initial conditions at $z = 200$ mm are the following: $T_r = 4000$ K, $T_e = 6700$ K, $T_v = 5500$ K, $N_e = 7.10^{11}$ cm^{-3}, and the velocity distribution is approximated by $v = 5000 \times (200/z)^{1/3}$ m/s. In order to reproduce the mass spectrometry measurements better, the molar fraction of the atomic species N and O had to be increased considerably (10% of the total sum of neutral species). This must certainly be due to atomic recombination reactions near the flat plate and inside the orifice that are not taken into account in the model. In this configuration, the agreement is correct between experimental and numerical results, except for N^+ and N_2^+, whose measured slopes as a function of z decrease very sharply. Comparing each production rate w_j of a reaction j, we find that w_j is greater than or about equal to 1 for only eight of them. These eight reactions are now presented in the forward (endothermic) sense; but in all cases the sign of w_j indicates that the reverse process is dominant:

Neutral exchange reactions

$$N_2 + O \rightleftarrows NO + N$$

$$NO + O \rightleftarrows O_2 + N$$

Associative ionization/dissociative recombination reactions

$$N + O \rightleftarrows NO^+ + e$$

$$O + O \rightleftarrows O_2^+ + e$$

$$N + N \rightleftarrows N_2^+ + e$$

Electron ionization/ionic recombination reactions

$$O + e \rightleftarrows O^+ + e + e$$

$$N + e \rightleftarrows N^+ + e + e$$

Charge transfer reaction

$$NO^+ + O_2 \rightleftarrows O_2^+ + NO$$

Except for the recombination effects, the differences between the experimental and numerical data may be due to 1) uncertainties in the measurement of the temperatures, of the electron density, and of the molar fraction of 11 species, which determine the initial conditions; 2) the influence of other species measured by mass spectrometry as H_2O, OH, H_2O^+, etc., coming from the residual gas or as N_2O and N_2O^+ formed in the plasma. The importance of the external gas seems to be proved by the decrease of the velocity flow v with z, but other parameters as viscosity and expansion of the jet due to diffusion may be involved in the $v(z)$ profile; 3) errors in the correction factors described above, which were used for data mass analysis; 4) hydrodynamic instabilities of the plasma flow, which affect especially the measurement of ionic species present in relatively small quantities in the plasma flow; and 5) the choice of a theoretical monodimensional model, which does not account for radial diffusive effects.

Conclusions

Preliminary investigations have been made concerning the measurements at a stagnation point in an air plasma. Axial electron density and temperature distributions have been deduced from the analysis of double-probe characteristics using Laframboise calculations coupled with the algebra formalism

of Peterson and Talbot. The validity of the theory used is well-proven by the very good fit between experimental and theoretical probe characteristics. Neutral particle and ion distributions from mass spectrometry measurements along the jet axis have been obtained. The comparison between experimental data and a numerical simulation using a Park model for air, including 11 species and a set of measured parameters, shows a qualitative agreement with respect to the majority of the species involved, provided that the molar fractions of N and O are raised considerably. From these results, it seems clear that the absence of atomic species coming from the plasma flow, in the mass spectra, must be due to recombination reactions inside the sampling orifice of the mass analyzer, as well as close to the catalytic flat plate. Further investigations are planned by mass spectrometry, and particular attention will be paid to the definition of a new sampling device, in order to minimize the recombination effects.

References

[1]Blackwell, H. E., and Scott, C. D., "Measured Rotational and Vibrational Temperature Differences in Arc Jet Shock Layers," AIAA Paper 92-3030, July 1992.

[2]Laure, S. H., Auweter-Kurtz, M., Fasoulas, S., Habiger, H., and Röck, W. R., "The IRS Plasma Wind Tunnels as a Tool for the Investigation of Planet Entry Missions," AIAA Paper 92-3886, July 1992.

[3]Moss, J. N., Cuda, V., and Simmonds, A. L., "Nonequilibrium Effects for Hypersonic Translational Flows," AIAA Paper 87-0404, Jan. 1987.

[4]Bussing, T. R. A., and Eberhardt, S., "Chemistry Associated with Hypersonic Vehicles," AIAA Paper 87-1292, June 1987.

[5]Sharma, S. P., and Gillepsie, W., "Nonequilibrium and Equilibrium Shock Front Radiation Measurements," *Journal of Thermophysics and Heat Transfer*, Vol. 5, No. 3, 1991, pp. 257–265.

[6]Chiroux de Gavelle de Roany, A., Flament, C., Rich, J. W., Subramaniam, V. V., and Warren, W. R., Jr, "Strong Vibrational Nonequilibrium in Supersonic Nozzle Flows," *AIAA Journal*, Vol. 31, No. 1, 1993, pp. 119–128.

[7]Röck, W. R., Auweter-Kurtz, M., Dabala, M., Früholz, P., Habiger, H., and Laure, S., "Experimental Simulation of the Entry of Huygens into the Titan Atmosphere for the Thermal Protection Qualification," 44th Congress of the International Astronautical Federation, Graz, Austria, Oct. 1993.

[8]Cernogora, G., Hochard, L., Dudeck, M., Lasgorceix, P., and Lago, V., "Vibrational Temperatures Measurements in Arc Jets," AIAA Paper 93-3229, July 1993.

[9]Lasgorceix, P., Lago, V., and Dudeck, M., "Fluxmètrie dans un Jet Raréfié de Plasma d'Air," *International Communications in Heat and Mass Transfer*, Vol. 20, No. 6, 1993, pp. 901–908.

[10]Lasgorceix, P., "Mise au Point d'un Ensemble Expérimental d'Analyse de Jets de Plasma d'Arc Raréfiés. Application à un Jet de Plasma d'Azote," Univ. of Paris-Sud, Thesis, Orsay, France, 1989.

[11]Peter, G., and Höfler, K., "Mass and Energy Analysis of Ions from Plasmas," *Journal of Vacuum Science and Technology*, Vol. A5, No. 4, 1987, pp. 2285–2289.

[12]Laframboise, J. G., "Theory of Spherical and Cylindrical Langmuir Probes in a Collisionless Maxwellian Plasma at Rest," Univ. of Toronto, Inst. for Aerospace Studies, Rept. 100, Toronto, Ontario, Canada, 1966.

[13]Peterson, E. W., and Talbot, L., "Langmuir Probe Response in a Turbulent Plasma," *AIAA Journal*, Vol. 8, No. 8, 1970, pp. 1391–1398.

[14]Peterson, E. W., and Talbot, L., "An Analytical Description of the Free-Molecule Cylindrical Electrostatic Single-Probe and Double-Probe Measurements," Aeronautical Sciences Div., Rept. AS-69-12, Univ. of California, Berkeley, CA, 1969.

[15]Johnson, E. O., and Malter, L., "A Floating Double Probe Method for Measurements in Gas Discharges," *Physical Review*, Vol. 80, No. 1, 1950, pp. 58–68.

[16]Schönemann, A., and Auweter-Kurtz, M., "Mass Spectrometric Measurements of a N_2/O_2 Plasma Flow," International Conf. on Phenomena in Ionized Gases, ICPIG XXI, Bochum, Germany, 1993.

[17]Schönemann, A., and Auweter-Kurtz, M., "Characterization of Nitrogen and Air Plasma Flows by Mass Spectrometry," 11th International Symposium on Plasma Chemistry, ISPC 11, Loughborough, England, UK, 1993.

[18]Schönemann, A., Auweter-Kurtz, M., Habiger, H. A., Sleziona, P. C., and Stöckle, T., "Experimental and Numerical Investigation of the Influence of Argon Used as Protection Gas in a Reentry Simulation Device," AIAA Paper 93-2829, July 1993.

[19]Robin, L., "Etude Cinétique et Interaction de Paroi dans un Jet de Plasma d'Azote Basse Pression," M.S. Thesis, Univ. of Rouen, France, 1989.

[20]Park, C., "Nonequilibrium Hypersonic Aerothermodynamics," Wiley-Interscience, New York, 1990.

[21]Park, C., and Lee, S. H., "Validation of Multi-Temperature Nozzle Flow Code NOZNT," AIAA Paper 93-2862, July 1993.

[22]Tardy, P., "Etude et Mise au Point d'un Dispositif Expérimental de Mesure de la Vitesse d'un Jet de Plasma Raréfié," M.S. Thesis, Univ. of Paris-Sud, Orsay, France, 1991.